Direct simulation Monte Carlo investigation of the Rayleigh-Taylor instability

M. A. Gallis,[1,*] T. P. Koehler,[1] J. R. Torczynski,[1] and S. J. Plimpton[2]
[1]*Engineering Sciences Center, Sandia National Laboratories, P.O. Box 5800, Albuquerque, New Mexico 87185-0840, USA*
[2]*Computing Research Center, Sandia National Laboratories, P.O. Box 5800, Albuquerque, New Mexico 87185-1316, USA*
(Received 4 March 2016; published 31 August 2016)

The Rayleigh-Taylor instability (RTI) is investigated using the direct simulation Monte Carlo (DSMC) method of molecular gas dynamics. Here, fully resolved two-dimensional DSMC RTI simulations are performed to quantify the growth of flat and single-mode perturbed interfaces between two atmospheric-pressure monatomic gases as a function of the Atwood number and the gravitational acceleration. The DSMC simulations reproduce many qualitative features of the growth of the mixing layer and are in reasonable quantitative agreement with theoretical and empirical models in the linear, nonlinear, and self-similar regimes. In some of the simulations at late times, the instability enters the self-similar regime, in agreement with experimental observations. For the conditions simulated, diffusion can influence the initial instability growth significantly.

DOI: 10.1103/PhysRevFluids.1.043403

I. INTRODUCTION

The Rayleigh-Taylor instability (RTI) evolves at the unstable interface of two fluids of different densities subjected to a common acceleration normal to the interface. In this situation, small interfacial perturbations evolve into mushroomlike structures with wavelength λ and amplitude a, which increase as time progresses. The RTI is observed in flows with widely differing length scales: up to light-years for a supernova [1] and down to millimeters for inertial confinement fusion (ICF) [2]. In fact, failure to achieve ignition at the National Ignition Facility may be caused by RTI mixing that limits the radial compression by prematurely mixing the fuel and reducing heating efficacy at the time of maximum compression [3].

Taylor [4] conducted the original theoretical study of the RTI, and Lewis [5] conducted the companion experimental study. Chandrasekhar [6] subsequently noted that Rayleigh [7] treated fundamentally the same problem in his earlier work on the equilibrium of a fluid of variable density under gravitational acceleration. Since then, many sophisticated theoretical and experimental studies have been conducted to quantify the behavior of the RTI. Extensive reviews of the more recent research on the RTI can be found in the works of Sharp [8], Kull [9], and Abarzhi [10]. The development of the initial stage of the RTI is described by the theory of Taylor [4]. However, due to the complexity of the latter stages of the RTI, a complete understanding of the physical phenomena involved, such as secondary instabilities, failure modes, and the stabilization of the mixing process [10], has not been achieved to date.

The RTI is often described [11–13] as having three fundamentally different phenomenological stages of mixing: linear, nonlinear, and turbulent. In the first stage, small initial perturbations on the interface grow exponentially. In this stage, the growth dynamics can be described by two length scales: the perturbation amplitude in the acceleration direction and the perturbation wavelength, which is related to the mode of fastest growth (i.e., the most unstable wavelength). In the second stage, larger coherent structures appear as smaller disturbances interact and merge. These interactions occur when the perturbation amplitude becomes comparable to the perturbation wavelength. In this

*magalli@sandia.gov

stage, the amplitude growth follows a power law with time. In the third stage, secondary instabilities such as the Kelvin-Helmholtz instability develop and eventually break up the coherent structures, which results in turbulent and chaotic mixing of the fluids.

The details of the evolution of the RTI clearly depend on the properties of the two fluids. The effects of compressibility, surface tension, diffusivity, and viscosity on the initial exponential growth rate of small-amplitude perturbations have been studied extensively [14–17]. By broadening the density transition between the gases [15], viscosity and diffusivity inhibit small-wavelength perturbations from growing, thereby allowing a particular wavelength (the most unstable wavelength λ_m) to emerge, whose growth outpaces the growth of other wavelengths. Diffusion can also reduce the effective buoyant forces, thus slowing down the mixing process [16]. As a result, for an initially flat interface, the most unstable wavelength has the following form [8]:

$$\lambda_m \approx 4\pi(\nu^2/Ag)^{1/3}, \tag{1}$$

where g is the gravity (acceleration) to which the domain is subjected, ν is the mean kinematic viscosity of the two fluids, A is the Atwood number, and ρ_H and ρ_L are the densities of the heavy and light fluids, respectively:

$$A = \frac{\rho_H - \rho_L}{\rho_H + \rho_L}. \tag{2}$$

Other factors that have been shown to influence the growth of the instability include the dimensionality of the flow, the time dependence of gravity, and boundary effects [8–11].

Nondimensionalization and scaling have been applied to provide insight into the effects of various phenomena on the evolution of the RTI. Wei and Livescu [17] proposed using a perturbation Reynolds number Re_p to describe the evolution of the RTI:

$$\mathrm{Re}_p = \frac{\lambda}{\nu}\sqrt{\frac{A}{1+A}g\lambda}. \tag{3}$$

They found that the growth at low Re_p is dominated by viscous diffusion but that the growth at high Re_p is dominated by complex vortical motions. Here Re_p quantifies the effect of diffusivity by introducing a cutoff wavelength below which the instability does not develop, even at late times. It is also common to utilize length and time scales based upon gravity and the initial perturbation wavelength as a means to analyze data [11]. A typical time scale associated with the growth of the instability is

$$\tau \sim 1/\sqrt{Agk}, \quad k = 2\pi/\lambda. \tag{4}$$

In this paper Bird's direct simulation Monte Carlo (DSMC) method [18,19] of molecular gas dynamics is used to investigate the growth of the RTI. In distinction to most simulation methods that have been applied to the RTI [10], the DSMC method uses large numbers of computational molecules (called particles or simulators) to represent a gas flow. These particles move, collide with each other, and reflect from walls with the same statistics produced by actual gas molecules. Being a molecular method, the DSMC method straightforwardly treats multiple gas species. Macroscopic flow properties are found by averaging the properties of the particles within each cell over some period of time, which can be short compared to flow time scales. Current massively parallel computational platforms have now made it possible to track very large numbers of particles for long times in macroscopic domains, which enables the DSMC method to simulate hydrodynamic flows [20]. Thus, molecular methods like the DSMC method are becoming increasingly popular for investigating the effects of viscosity and diffusivity in ICF applications, which are known as kinetic or ion-kinetic effects. See the recent paper by Larroche *et al.* [21] for an in-depth discussion of this topic.

Fully resolved two-dimensional DSMC RTI simulations are performed for monatomic gases at essentially atmospheric conditions. In the first series of simulations, the Atwood number A is fixed by using argon and helium, and the gravitational acceleration g is fixed, but the initial perturbation

wavelength λ is varied. In the second series of simulations, the Atwood number A is again fixed by using argon and helium, and the initial perturbation wavelength λ is fixed, but the gravitational acceleration g is varied. In these two series, since the gases are fixed, the viscosity and the diffusivity are fixed. In the third series of simulations, the gravitational acceleration g and the initial perturbation wavelength λ are both fixed, but the Atwood number A is varied by using different combinations of gases. In this series, since the gases are varied, the viscosity and the diffusivity are varied along with the Atwood number, so the effect of Atwood number is not isolated in this series. It is in principle possible to specify DSMC gas parameters that would fix the transport properties while varying the Atwood number [18,19]. However, such "artificial" gases are not employed here. These three series of simulations employ an initial perturbation amplitude a_0 that is 1% of the initial perturbation wavelength λ. The first case for each of these three series is the same and thus is the baseline case for comparison. In the fourth series of simulations, the conditions are the same as in the third series except that the initial interface is molecularly flat (i.e., an initial amplitude a_0 of zero).

Amplitude-growth results obtained from these DSMC simulations are compared with linear and nonlinear theoretical results and experimental results. The trends with wavelength, gravitational acceleration, and Atwood number are as expected, although differences from theoretical predictions due to diffusion are observed. When diffusion effects are small, the simulations produce the most unstable wavelength predicted by theory. The onset of self-similarity for mixing at late times is also observed in some cases.

II. THEORETICAL MODELS

As described in the Introduction, numerous efforts have been made to characterize, predict, and describe the growth of the RTI. The early-time growth stage of the instability is well represented by an exponential derived from linear stability theory. The nonlinear growth stage of the instability has been the subject of multiple theoretical attempts to accurately represent the growth of coherent bubble and spike structures as the instability transitions to a self-similar, turbulent mixing regime. In the turbulent mixing regime, the width of the mixed layer is described by a simple quadratic expression.

Linear stability theory determines when a flow is unstable to infinitesimal disturbances. Infinitesimal disturbances are always present, even for a molecularly flat surface. As mentioned in the Introduction, Rayleigh [7] first studied the stability of the interface between two fluids under the influence of a gravitational field and Taylor [4] subsequently added an acceleration induced by pressure gradients. According to Taylor's linear stability theory, initial perturbations with small wavelengths grow faster, where a is the perturbation amplitude:

$$a = a_0 \cosh(t\sqrt{Agk}), \quad k = 2\pi/\lambda. \tag{5}$$

Equation (5) indicates that smaller wavelengths have larger growth rates and that, for times before viscosity and diffusivity become important, the initial growth scales as gt^2. When the effects of viscosity and diffusivity become significant, the instability amplitude is modified [15]:

$$a = a_0 \exp([(Agk/\psi + \nu^2 k^4)^{1/2} - (\nu + D)k^2]t), \tag{6}$$

where $k = 2\pi/\lambda$ is the wave number for wavelength λ, ν is the kinematic viscosity, D is the diffusivity, and ψ is a function of the Atwood number A. In this case, the exponent in Eq. (6) has a maximum for some particular wavelength, the most unstable wavelength λ_m.

Experiments have confirmed that linear theory correctly accounts for the early-time evolution of the instability amplitude [8–10]. However, at later times, where $ka \sim 1$, the flow behaves in a more complicated way, so a nonlinear stability approach or an empirical analysis is required. Building on an earlier model of Layzer [22] and its extension by Goncharov [23], Mikaelian [24] developed a model for the bubble amplitude a^b:

$$a^b(A) = a_0 + \left(\frac{3 + A}{3(1 + A)k}\right) \ln\left(\cosh\left[t\frac{\sqrt{6gkA(1 + A)}}{(3 + A)}\right]\right). \tag{7}$$

It should be noted that in order to extend the model of Layzer [22] to a two-fluid system, Goncharov disregarded the boundary condition at one of the outer boundary of domain [23]. As a result, a spurious uniform pipe-flow-like velocity field was produced in the light fluid far from the interface in the nonlinear regime [23]. Such a velocity field is not generally observed in RTI experiments and simulations. Thus, this type of model can be applied only in the vicinity of the interface and far away from the boundaries of the domain, as Goncharov noted [23].

Mikaelian proposed an empirical correlation for the spike amplitude a^s that interpolates between the spike amplitudes at Atwood numbers of 0 and 1:

$$a^s(A) = a^b(A)\left(1 + [0.4 + 0.6A^{10}]\left[\left(\frac{a^s(1)}{a^b(A)}\right)^A - 1\right]\right). \tag{8}$$

This empirical correlation is based on a large number of experimental and numerical results, the review of which is outside the scope of this paper. As expected, a^s approaches a^b for small A but increases with A to become 4–5 times a^b. While sophisticated theoretical approaches developed in recent decades have expanded our understanding of the RTI, especially for the early stages of the instability development, multiple issues, such as RTI dynamics in diffusive and stratified media [10], still remain areas of active research.

As the RTI develops further, the coherent structures begin to break down and a self-similar turbulent mixing layer evolves. The existence of a self-similar regime for the RTI was first discussed by Fermi and von Neumann [25] and is the basis of early turbulent mixing models [26]. In the turbulent regime, experimental data suggest that the bubble and spike growth rates are both self-similar [13,27] and can be described by a relatively simple model,

$$a^{b,s} = \alpha^{b,s} A g t^2, \tag{9}$$

where α^b is a constant, usually between 0.03 and 0.07, that is independent of A but where α^s is not constant and depends on A. For the self-similar solution to be applicable, the instability amplitude must be greater than the viscous and diffusion scales. In practical terms, this means that the total instability growth $h = a^b + a^s$ must satisfy the condition

$$\lambda_m \ll h \ll L, \tag{10}$$

where L is the size of the physical domain.

Although the RTI has been treated successfully in the hydrodynamic regime, recently, with the advent of supercomputers, RTI flow fields have been simulated using molecular methods. The applicability of molecular methods to instability simulations has been investigated by Kadau *et al.* [28,29], Barber *et al.* [30], and Mościński *et al.* [31]. Their results suggest that, for liquids, molecular-dynamics approaches can qualitatively and quantitatively describe the development of the RTI. In their results, the three stages of the instability are clearly observed as time progresses. The small initial perturbations evolve into larger spikes and bubbles, some showing turbulent shedding of vortices and eventually breaking completely apart. Kadau *et al.* [28,29] further showed good agreement with experimental data for spike positions and velocities. Using a particle-based, kinetic Monte Carlo method, Sagert *et al.* [32] also demonstrated good agreement with growth rates in the linear regime.

Although most studies have focused on the RTI in liquids and plasmas, the RTI is observed in gases as well. For gases, interdiffusion of the two species can cause the growth rate to differ from models that assume a sharp interface. A physically realistic representation of the growth rate must include the fact that the interface is continuous and evolving with time due to diffusion, which competes with the effect of acceleration. Abarzhi [10] suggests that, for compressible and miscible fluids, if the interface is defined as the region of steep density gradients, then kinetic processes at the molecular scale should be considered.

III. NUMERICAL METHOD

As mentioned in the Introduction, Bird's DSMC method [18,19] is a molecular technique for simulating gas flows when the mean free path is much larger than the molecular diameter, which is typically the case. The DSMC method employs a particle-based stochastic algorithm to solve the Boltzmann equation by approximating the continuous molecular velocity distribution function with a discrete number of computational molecules [18,19]. Each computational molecule, or particle, typically represents a large number of real molecules and these particles move, collide with other particles, and reflect from boundaries. The physical domain is discretized into a set of cells. A time-splitting scheme is used that consists of a move operation, during which particles translate ballistically over time step Δt, followed by a collide operation, during which pairs of particles within the same cell are randomly selected for collision. Macroscopic gas properties are determined by sampling the properties of the particles resident in a cell at a particular time. The standard DSMC method executes each of these operations once per time step in the order move, collide, and sample.

Historically, the DSMC method has been very successful in the study of rarefied, high-speed flows typical of aerospace engineering [33]. The validity of the DSMC method for this class of problems has been firmly established by comparisons to experimental measurements [34] and molecular-dynamics simulations [35]. Wagner [36] proved that DSMC simulations approach solutions of the Boltzmann equation for monatomic molecules in the limit of vanishing discretization and statistical errors. Recently, Gallis *et al.* [37] reported highly refined DSMC simulations of the Fourier heat-flow problem and observed excellent agreement ($\sim$0.2%) between their calculated bulk viscosity [37], thermal conductivity [38], diffusivity [39], and the Chapman-Enskog (CE) infinite-approximation results [40]. They also showed that the DSMC-calculated velocity distribution function, as quantified by its Sonine-polynomial coefficients, is in excellent agreement with the CE theoretical values [40] for near-equilibrium flows and with theoretical values from the moment-hierarchy method for highly nonequilibrium flows [41].

In common with other molecular methods, the DSMC method has advantages and disadvantages relative to typical hydrodynamic simulation methods. A major advantage is that the DSMC method is not limited to near-equilibrium conditions and small gradients. More specifically, the DSMC method inherently accounts for both near-equilibrium transport (viscosity, thermal conductivity, and mass diffusivity) and nonequilibrium phenomena (thermal and pressure diffusion). A major disadvantage of the DSMC method is that the particles intrinsically produce significant statistical noise. When each particle represents a single actual molecule, the DSMC method exactly reproduces the fluctuations in an equilibrium gas [42], which are typically extremely small. Otherwise, the variances of the fluctuations in a DSMC simulation are the actual variances multiplied by the number of actual molecules represented by each particle (i.e., the simulation ratio).

The extremely large computational effort required to achieve an acceptable signal-to-noise ratio has generally prevented the use of the DSMC method and other molecular methods in the hydrodynamic regime. Thus, up to the present, the inherent capability of the DSMC method to simulate macroscopic hydrodynamic phenomena at the molecular level has rarely been exercised [30,32]. Another, more subtle issue arises from fluctuation correlations [43]. At equilibrium, fluctuations of conjugate hydrodynamic quantities are uncorrelated. However, out of equilibrium, these quantities can be correlated, and these correlations can introduce a statistical bias. Despite these difficulties, the Richtmyer-Meshkov instability, often considered to be like the RTI with impulsive acceleration, has been successfully simulated by the DSMC method [20].

The aim of this work is to study the development of the RTI in gases at the molecular level and in particular to study the effect of gas diffusivity on the growth of the instability. Diffusivity is often considered of lesser importance and therefore neglected in hydrodynamic descriptions. However, diffusivity may be the primary growth driver in initially flat interfaces and a significant contributor in initially perturbed interfaces in millimeter-scale domains, similar to those encountered in ICF. More specifically, the three-dimensional DSMC code SPARTA [44], developed to be highly efficient on massively parallel computers, is used to simulate the RTI for two-dimensional perturbations in

TABLE I. Properties of pure gases at STP. The DSMC method automatically computes values for mixtures.

Gas	m (kg)	T (K)	p (Pa)	ρ (kg/m^3)	μ (Pa.s)	ν (m^2/s)
He	6.65×10^{-27}	273.15	101325	0.179	1.865×10^{-5}	10.4×10^{-5}
Ne	33.5×10^{-27}	273.15	101325	0.900	2.975×10^{-5}	3.31×10^{-5}
Ar	66.3×10^{-27}	273.15	101325	1.781	2.117×10^{-5}	1.19×10^{-5}
Kr	139.1×10^{-27}	273.15	101325	3.737	2.328×10^{-5}	0.62×10^{-5}

millimeter-scale domains for atmospheric-pressure gases with various Atwood numbers (0.32–0.82) and gravity $g = 10^7 - 10^8$ m/s^2. Simulations are performed on Sequoia, an IBM Blue Gene/Q supercomputer at Lawrence Livermore National Laboratory, using up to 1.57 million cores for up to 30 h.

IV. NUMERICAL ANALYSIS DETAILS

The DSMC code SPARTA [44,45] is used to simulate the RTI at the interface separating two gases experiencing a constant acceleration. The gases are dilute and obey the perfect-gas equation of state and are taken to have constant values of the specific heat ratio γ. These approximations are reasonable for the modest temperatures and pressures considered here.

Four gases are used: helium, neon, argon, and krypton. For each gas combination investigated (Ar/He, Ar/Ne, and Kr/Ne), the initial conditions consist of the heavier gas on top of the lighter gas. The lighter gas is initially at 273.15 K and 101325 Pa (STP) at the bottom of the domain. Throughout the rest of the domain, both gases are initially at 273.15 K and have initial density distributions corresponding to hydrostatic equilibrium at the given gravity value. Table I shows the properties of pure He, Ne, Ar, and Kr at STP [18,19]. The DSMC method automatically computes the properties of gas mixtures [18,19]. Ar/He simulations are performed for four gravity values: $g = \{1.0,0.5,0.3,0.1\} \times 10^8$ m/s^2. All other gas combinations are simulated only for a gravity value of $g = 10^8$ m/s^2.

For the baseline simulation, a 1 mm $\times$ 4 mm domain is used, and a sinusoidal perturbation with a wavelength of $\lambda = 1$ mm (equal to the domain width) and an amplitude $a_0 = \lambda/100$ is initially imposed on the interface at $y = 2$ mm. The domain is divided into 1.6 billion square cells with a side length of 50 nm, which is less than a mean free path at the interface for the gases considered. The domain is initialized in hydrostatic equilibrium with an average of 12.5 particles per cell, for a total of 20 billion particles. Due to the initial density gradient across the domain, most of the particles were concentrated at the lower half of the domain. With this particle density, the two-dimensional simulation could be considered as a thin (0.4-nm) three-dimensional domain in which each particle represents one real molecule. The molecular collisions are performed using the hard-sphere model with parameter values suggested by Gallis *et al.* [37]. The time step is 0.1 ns, which is less than both the mean collision time and the mean transit time of molecules in a cell. Based on these simulation parameters, the discretization error is estimated to be less than 2% [38].

The following boundary conditions are used in each simulation. Periodic boundary conditions are applied along the sides of the domain: Particles exiting the domain at one side reenter the domain from the opposite side with no change in properties. The top and bottom boundaries are diffuse walls: Incident particles are reflected such that statistically they are fully accommodated to the wall temperature, which is taken to be the initial gas temperature. This boundary condition ensures that the flow velocity vanishes far from the interface but does not vanish close to the interface, as in Layzer's model [22] and Goncharov's extension [23].

Mass is conserved throughout a simulation: No particles are added or removed from the domain, so the number of particles remains unchanged with time. At each time step, a small amount of downward momentum from gravity is added to each particle. The force corresponding to this

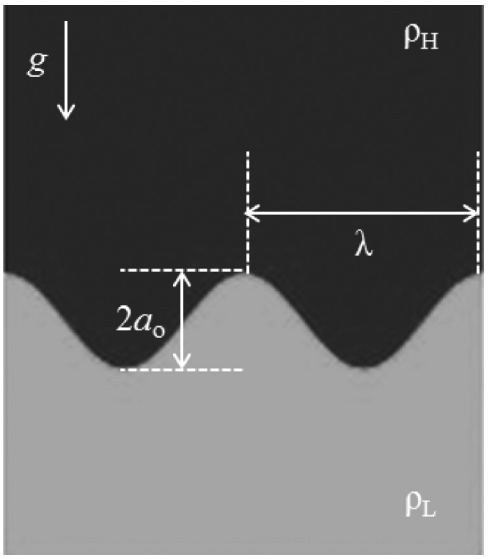

FIG. 1. RTI schematic diagram showing gas densities, gravitational acceleration, and perturbation wavelength and initial amplitude.

continual addition of momentum exactly counterbalances the pressure gradient from the hydrostatic density distribution used as the initial condition for a simulation. Besides energy changes due to gravity, particles also exchange small amounts of energy when reflecting from the top and bottom walls of the domain, as mentioned above.

Due to the magnitude of the data managed and processed by SPARTA at every time step, storage limitations and buffering restrictions required the data to be reduced prior to output for postprocessing and analysis. To accomplish this, we utilized *in situ* on-the-fly visualization capabilities in SPARTA to output images of the gas-species distributions in the domain. At predefined time steps, images of the majority-species field are created in which each cell of the domain is colored to represent the gas with the most molecules in it, as shown in Fig. 1. The cells could have been colored with other physical quantities, such as concentration, mass density, or a velocity component. However, only one field could be output for each of these simulations due to their size, so the majority-species field described above was selected because it reveals the bubbles and the spikes clearly and thus enables their growth rates to be determined accurately.

Through image analysis, each series of images is postprocessed to provide quantitative values for the instability growth. The bubble and spike peaks are defined to be the cells of one gas that have penetrated furthest into the cells of the other gas and their positions are determined for each image. The interface position is taken to be stationary in the middle of the domain.

V. RESULTS

In this section, DSMC simulations of two distinct RTI scenarios are presented. In the first scenario, an initial perturbation is imposed upon the interface with an amplitude $a_0 = \lambda/100$, so the instability grows initially in the linear regime and progresses into the early nonlinear regime. In the second scenario, the initial interface is flat (i.e., the amplitude is set to zero initially). At the molecular level, an interface cannot ever be mathematically flat. Thus, the effect of molecular fluctuations on instability growth is inherently observed. In both situations, DSMC results are obtained that can be quantitatively compared to the models discussed previously. In the cases presented here, the domains are long enough to prevent the top and bottom boundaries from interfering with the growth of the perturbation for the time considered.

TABLE II. Parameters for DSMC RTI simulations with various values of Atwood number A, gravity g, wavelength λ, and initial amplitude a_0. Here Re_p is the perturbation Reynolds number, $\lambda_{m,\mathrm{mean}}$ is the mean most unstable wavelength, and $\lambda_{m,\mathrm{light}}$ is the most unstable wavelength of the light gas.

Case	Gases	A	g (m/s^2)	λ (mm)	a_0 (μm)	Re_p	$\lambda_{m,\mathrm{mean}}$ (μm)	$\lambda_{m,\mathrm{light}}$ (μm)
1a	Ar/He	0.82	1.0×10^8	1.00	10.0	7486	26.9	80.1
1b	Ar/He	0.82	1.0×10^8	0.75	7.5	4863	26.9	80.1
1c	Ar/He	0.82	1.0×10^8	0.50	5.0	2647	26.9	80.1
1d	Ar/He	0.82	1.0×10^8	0.25	2.5	936	26.9	80.1
2a	Ar/He	0.82	1.0×10^8	1.00	10.0	7486	26.9	80.1
2b	Ar/He	0.82	0.5×10^8	1.00	10.0	5294	28.3	33.9
2c	Ar/He	0.82	0.3×10^8	1.00	10.0	4101	40.2	119.7
2d	Ar/He	0.82	0.1×10^8	1.00	10.0	2367	58.0	172.6
3a	Ar/He	0.82	1.0×10^8	1.00	10.0	7486	26.9	80.1
3b	Kr/Ne	0.61	1.0×10^8	1.00	10.0	12749	34.0	105.9
3c	Ar/Ne	0.32	1.0×10^8	1.00	10.0	5939	34.9	108.5
4a	Ar/He	0.82	1.0×10^8	1.00	0.0	7486	26.9	80.1
4b	Kr/Ne	0.61	1.0×10^8	1.00	0.0	12749	34.0	105.9
4c	Ar/Ne	0.32	1.0×10^8	1.00	0.0	5939	34.9	108.5

A. Initially perturbed interfaces

Table II presents the conditions for the DSMC RTI simulations. Four series of simulations are performed. In all four series, the domain width is equal to the perturbation wavelength λ. The first three series have an initial amplitude a_0 that is 1% of the perturbation wavelength λ and the first cases (a) of these three series are identical. The first series investigates the effect of perturbation wavelength λ for fixed Atwood number A and gravitational acceleration g. The second series investigates the effect of gravitational acceleration g for fixed Atwood number A and perturbation wavelength λ. The third series investigates the effect of gravitational acceleration g for fixed Atwood number A and perturbation wavelength λ. The fourth series is identical to the third series except that the initial amplitude a_0 is zero (the interface is initially molecularly flat). Since the product of the wave number $k = 2\pi/\lambda$ and the initial amplitude a_0 is much less than unity for these cases, the instability growth is initially linear (but ultimately becomes nonlinear).

1. Effect of perturbation wavelength

Figure 2 presents the mixing profiles for cases 1a–1d. As explained in the previous section, each computational cell is colored according to the majority species in the cell. While these cases begin as single-mode perturbations, cases 1a and 1b (the highest-Re_p cases) develop a multimode behavior as the interface evolves: Secondary bubbles and spikes form, grow with time, begin to interact, and eventually merge. In some cases, the stems of the spikes get thinner with time, leading to the shedding of droplets during the last stages of development. In cases 1a and 1b, the numbers of secondary bubbles and spikes that arise are proportional to the numbers that would be observed based on the most unstable wavelength determined from average gas properties, as previously suggested [11]. The secondary bubbles and spikes ultimately cause the single mode to become asymmetric.

Unlike cases 1a and 1b (the high-Re_p cases), cases 1c and 1d (the low-Re_p cases) evolve in a single-mode fashion until the bubbles and spikes eventually diffuse into each other. In cases 1c and 1d, secondary bubbles and spikes do not appear because the most unstable wavelength is greater than or comparable to the domain width. However, even in case 1d, for which the growth is predominantly diffusive, the initial perturbation grows and possesses some of the characteristics of the high-Re_p cases.

Figure 3 compares the bubble and spike amplitudes determined by DSMC simulations for cases 1a–1d to the results of linear theory and Mikaelian's model. The bubble amplitudes (the penetration

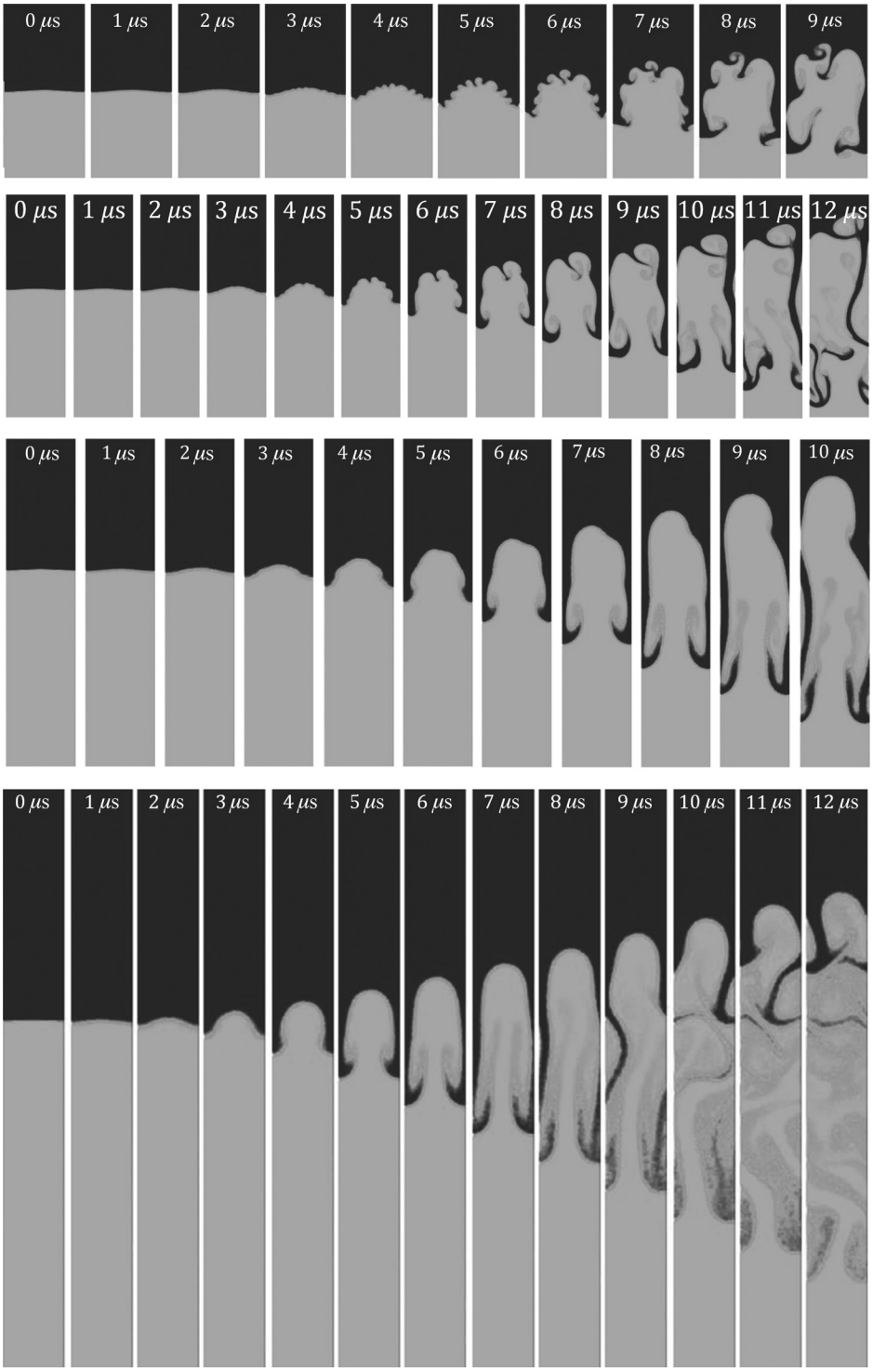

FIG. 2. DSMC RTI simulations for cases 1a–1d for the Ar/He gas combination ($A = 0.82$). The perturbation wavelength (from top to bottom) is 1.00, 0.75, 0.50, and 0.25 mm. The perturbation initial amplitude is 1% of the wavelength. Gravity equals 10^8 m/s^2. Domains are one wavelength wide.

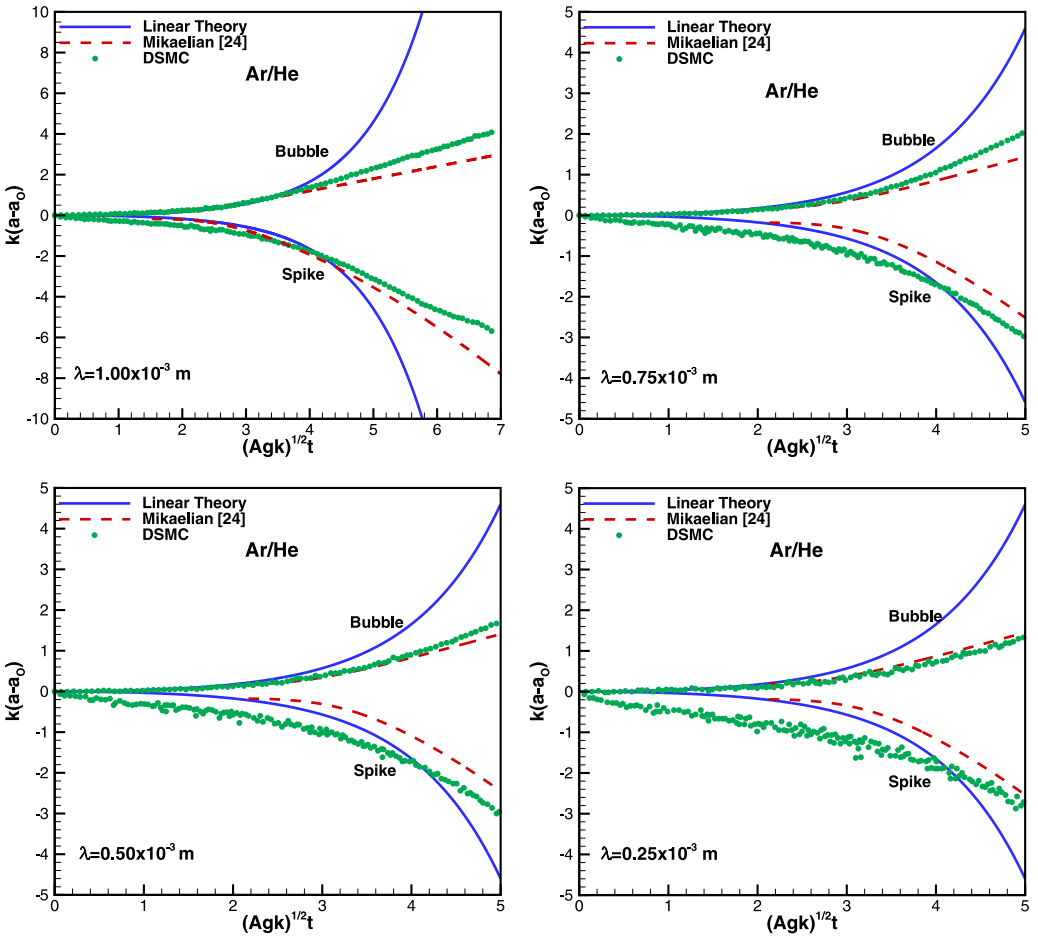

FIG. 3. Effect of wavelength on amplitude growth for cases 1a–1d in Fig. 2.

of the light gas into the heavy gas) are shown as positive values and the spikes (the penetration of the heavy gas into the light gas) are shown as negative values.

Thus, the total amplitudes are given by the separations between corresponding bubble and spike curves. As expected, the DSMC bubble growth is in excellent agreement with the linear theory until the amplitude grows to about twice the initial amplitude. At this point, the exponential growth is superseded by the power-law time dependence in the nonlinear regime [10]. After the initial linear regime, the DSMC growth rate follows this trend, which is significantly lower than the growth rate predicted by linear theory but very close to the growth rate predicted by Mikaelian's model.

The effect of diffusion is clearly demonstrated in the DSMC growth of the spike, for which appreciable departure from linear theory is observed even for case 1a (the highest-Re_p case). It is noted again that Mikaelian's model for spikes is a bridging function based on bubble growth. Bubble and spike growth rates are approximately equal only for vanishing Atwood numbers. Thus, unlike the bubble model, the spike model does not necessarily coincide with the DSMC results even initially.

The perturbation Reynolds number Re_p indicates the degree to which diffusion affects a perturbed interface. For example, diffusion becomes the dominant factor in case 1d, as expected for a low-Re_p case. This is not surprising considering that the initial amplitude and the initial wavelength for case 1d are only 25% of the corresponding values for case 1a.

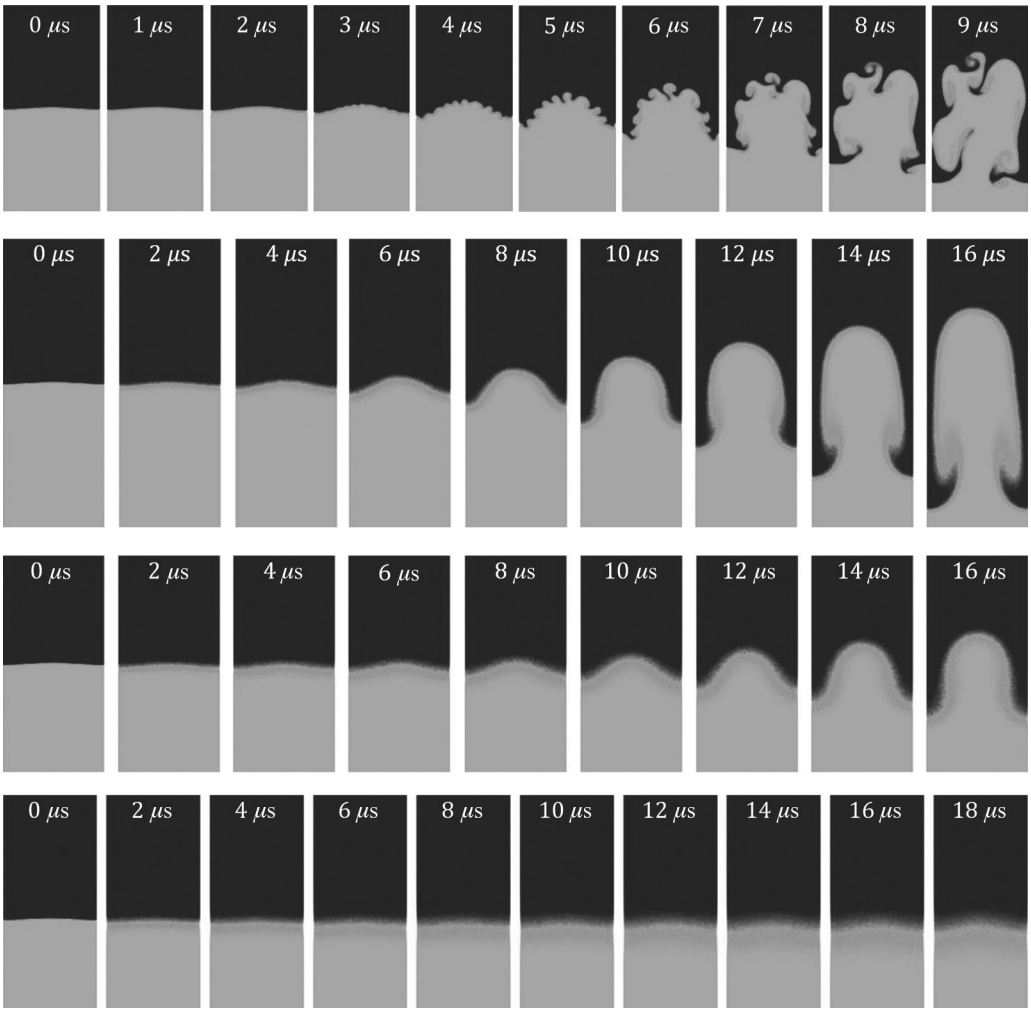

FIG. 4. DSMC RTI simulations for cases 2a–2d for the Ar/He gas combination ($A = 0.82$). The wavelength is 1.00 mm. The initial amplitude is 1% of the wavelength. Gravity equals (from top to bottom) $\{1.0,0.5,0.3,0.1\} \times 10^8$ m/s^2. Domains are one wavelength wide.

2. Effect of gravity

Cases 2a–2d illustrate the competition between the effects of buoyant convection and diffusion. For these cases, gravity is reduced from 10^8 m/s^2 to 10^7 m/s^2. As gravity is reduced, the Re_p value also decreases, indicating that diffusion should increasingly affect the instability growth. This trend is clearly seen when comparing frames at times with roughly constant values of gt^2, as suggested by Eq. (5): for example, from smaller to larger diffusion, case 2a at $t = 5\,\mu$s, case 2b at $t = 8\,\mu$s, case 2c at $t = 10\,\mu$s, and case 2d at $t = 18\,\mu$s.

Figure 4 presents the mixing profiles for cases 2a–2d. As gravity becomes weaker, the instability still grows, but the interface becomes less well defined due to diffusion. Moreover, secondary instabilities are suppressed because the most unstable wavelength increases. As the Re_p values for these cases suggest, diffusion becomes comparable to, and in case 2d greater than, the buoyant convection forces.

Figure 5 presents the amplitude as a function of time for cases 2a–2d. Even in case 2a (the highest-Re_p case), diffusion propagates the initial perturbation into the bulk gas until gravity accelerates the

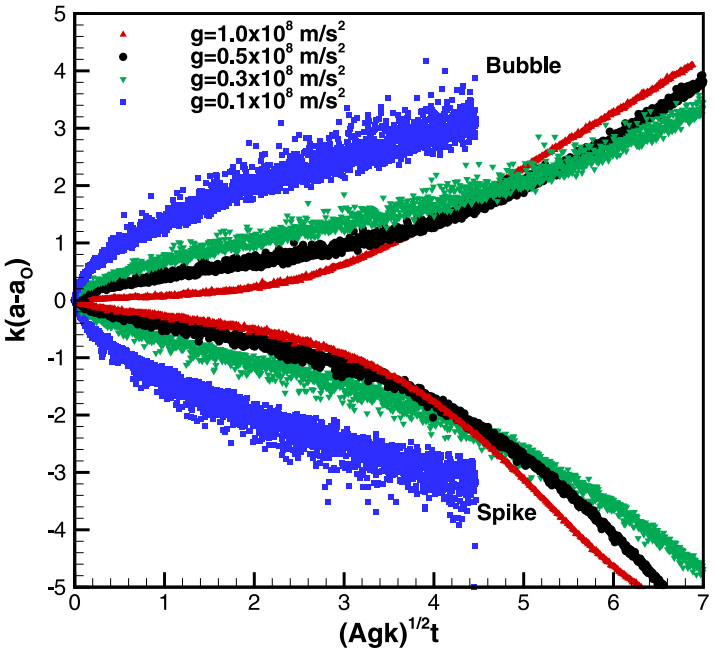

FIG. 5. Effect of gravity on amplitude growth for cases 2a–2d in Fig. 4.

flow such that the instability begins to develop. The domination of diffusion does not mean that the initial instability stops growing, even for the lowest gravity value, which is the most diffusive case, but diffusive growth is initially faster than convective growth.

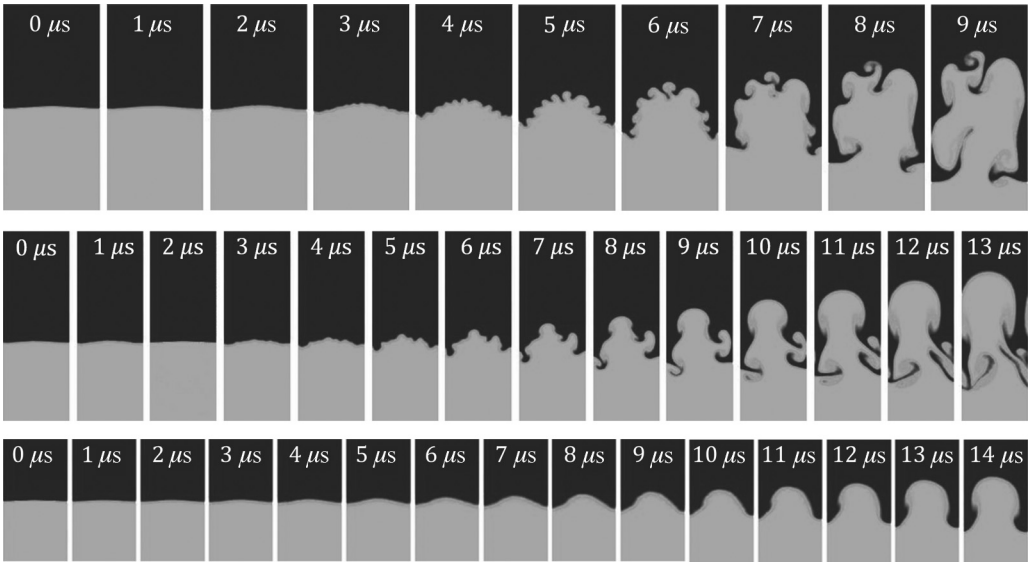

FIG. 6. DSMC RTI simulations for cases 3a–3c for the (from top to bottom) Ar/He ($A = 0.82$), Kr/Ne ($A = 0.61$), and Ar/Ne ($A = 0.32$) gas combinations. The wavelength is 1.00 mm. The initial amplitude is 1% of the wavelength. Gravity equals 10^8 m/s^2. Domains are one wavelength wide.

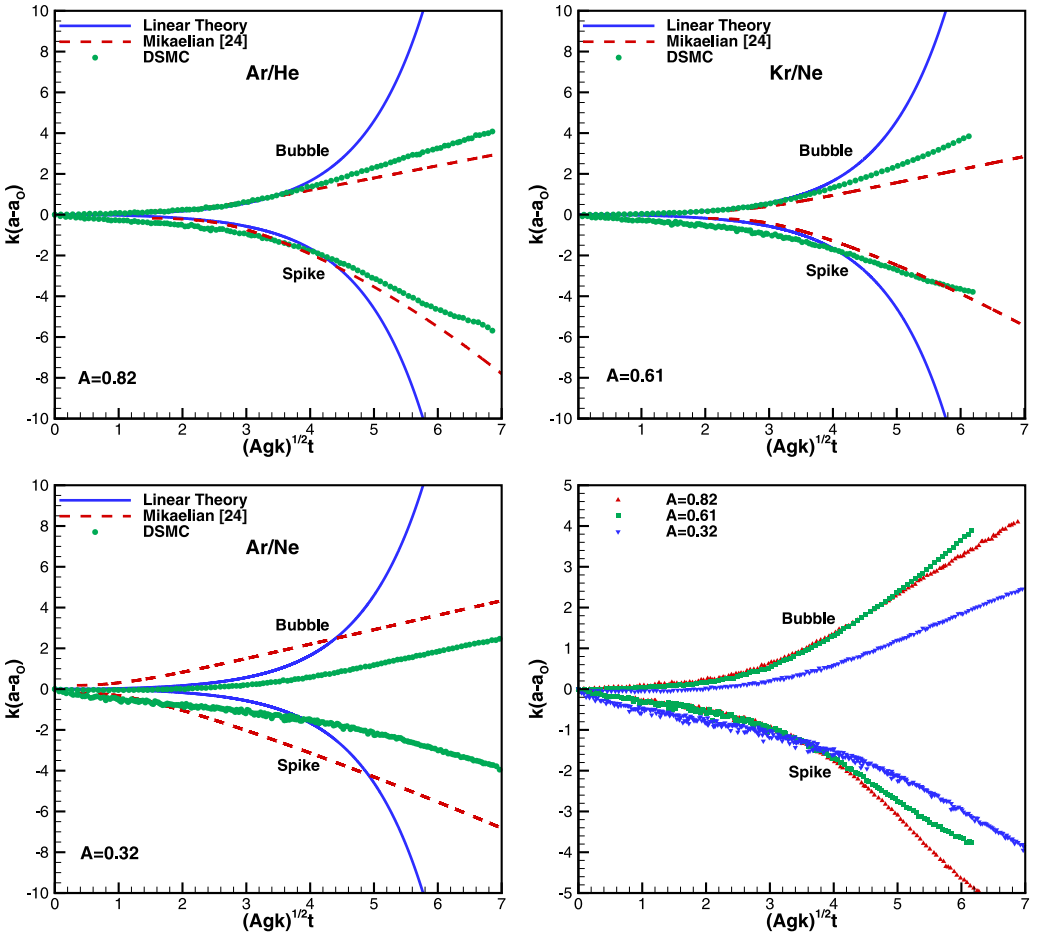

FIG. 7. Effect of Atwood number on amplitude growth for cases 3a–3c in Fig. 6.

3. Effect of Atwood number

Cases 3a–3c illustrate the effect of Atwood number on instability growth. The only difference between these individual cases is that different pairs of gases are used: Ar/He, Ar/Ne, and Kr/Ne. This leads to different Atwood numbers and different Re_p values and therefore to different values of the most unstable wavelength.

Figure 6 presents the mixing profiles for cases 3a–3c. Case 3a, the Ar/He combination, has the highest Atwood number. As the Atwood number decreases for cases 3b and 3c, the most unstable wavelength increases and the instability changes from multimode to single-mode growth. For these three cases, as the Atwood number decreases, Re_p first increases and then decreases. Thus, as mentioned earlier, the effect of Atwood number is not isolated from the effects of viscosity and diffusivity in this series. While it is in principle possible to specify DSMC gas parameters that would fix the transport properties while varying the Atwood number [18,19], such artificial gases are not employed here. Nevertheless, this series does indicate the qualitative effect of varying the Atwood number.

Figure 7 presents the amplitude as a function of time for cases 3a–3c along with the corresponding predictions of linear theory and Mikaelian's model. The comparison suggests that, in a similar fashion to what has been observed so far, the DSMC predictions are in reasonable agreement with theoretical predictions until diffusion becomes the dominant factor. It should be noted that, even in

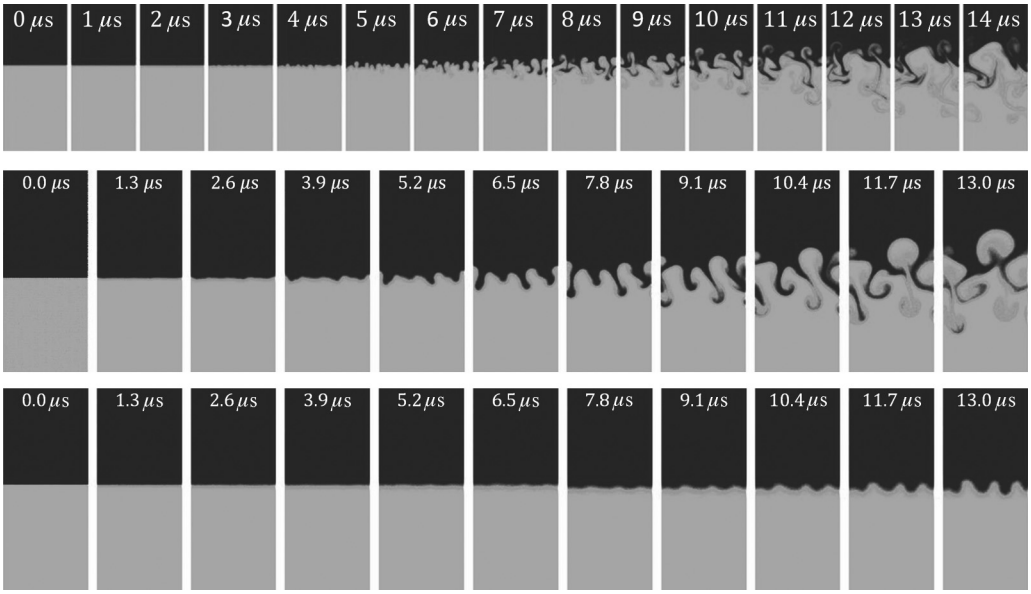

FIG. 8. DSMC RTI simulations for cases 4a–4c for the (from top to bottom) Ar/He ($A = 0.82$), Kr/Ne ($A = 0.61$), and Ar/Ne ($A = 0.32$) gas combinations. The domain width is 1.00 mm. The interface is initially flat. Gravity equals 10^8 m/s^2.

lowest-Re_p cases, the instability will eventually grow under the influence of gravity. However, by that time, diffusion has altered the amplitude and the wavelength of the interface so much that it is not described by the linear theory for an initially thin interface.

The bottom right plot in Fig. 7 presents the nondimensionalized instability growth for cases 3a–3c of Fig. 6. In agreement with expectations, the nondimensionalization suggests that the instability follows a universal behavior for high enough Re_p values. The differences between the cases simulated here become more pronounced in the nonlinear regime.

B. Flat interface

One of the advantages of studying the RTI at the molecular level is that molecular techniques can initialize a simulation with a molecularly flat interface. This initial condition is hard, if not impossible, to achieve experimentally. Since fluctuations are absent, a simulation using a typical hydrodynamic method must be initialized with an artificially perturbed interface, often using the most unstable wavelength. In a molecular simulation, fluctuations excite all possible interfacial modes in a random fashion. In their molecular-dynamics simulations initialized with a flat interface, Kadau *et al.* [28] observe that the unstable modes grow on average according to the predictions of linear stability theory.

The simulations of cases 4a–4c are identical to those of cases 3a–3c except that they are initialized with flat interfaces. Although the interface is macroscopically flat, it is perturbed microscopically on the length scale of interparticle separations. As a result, in the absence of a macroscopic perturbation, molecular fluctuations become important to the development and growth of the instability. In this situation, linear growth theory would predict no growth because macroscopically the perturbation amplitude is zero. However, as already observed, molecular fluctuations create a spectrum of perturbations. Perturbations with wavelengths near the most unstable wavelength will grow the most quickly. However, if no unstable wavelengths are produced, the interface will grow only by diffusion.

Figure 8 presents the mixing profiles for cases 4a–4c. Each of these cases has an initially flat interface (i.e., no perturbation wavelength is prescribed), so a spectrum of wavelengths can emerge in the flow field. Kadau *et al.* [28] point out that, as expected, although fluctuations excite all possible

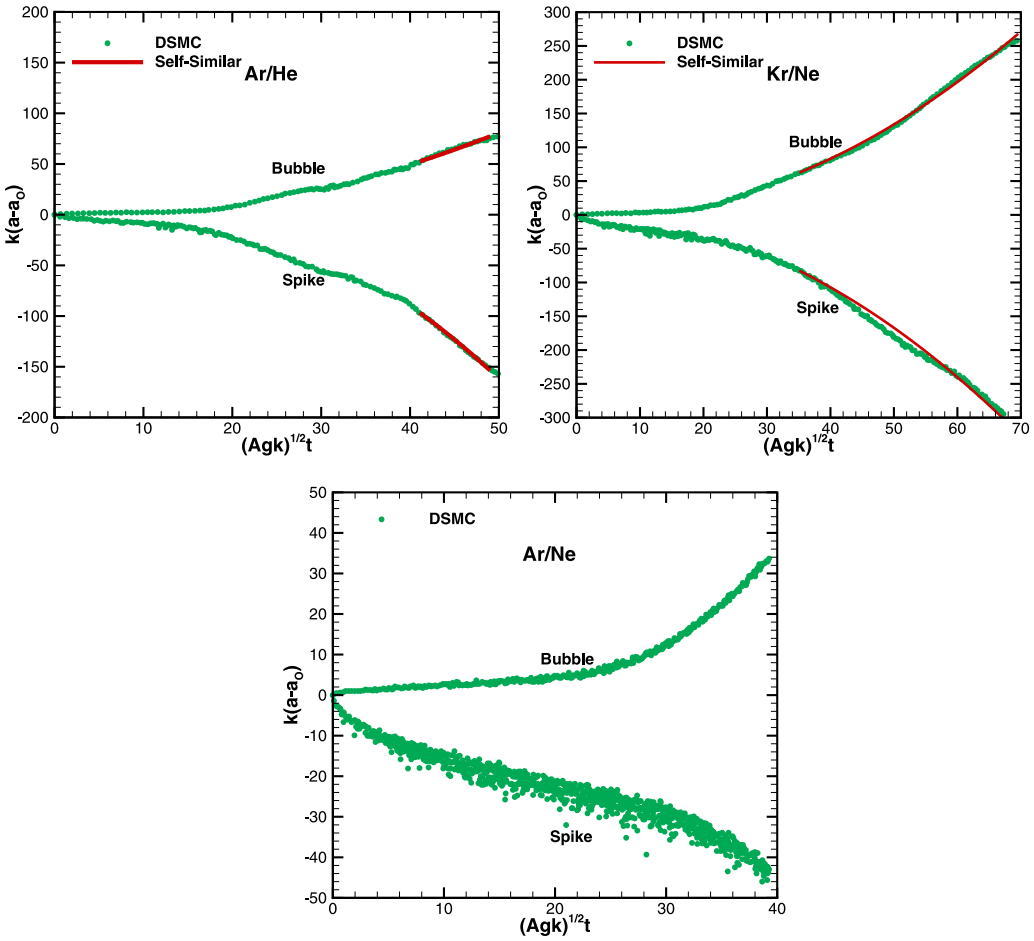

FIG. 9. Effect of Atwood number on amplitude growth for cases 4a–4c in Fig. 8, which have initially flat interfaces.

interfacial modes, the modes near the most unstable wavelength soon dominate. The interface grows as the emerging bubbles and spikes become longer, begin interacting with each other, and eventually merge, which results in chaotic mixing. As in cases 3a-3c, which have initially perturbed interfaces, the dominant wave number of the instability is approximately equal to the most unstable wave number in the light gas (see Table II).

Unlike deterministic computational-fluid-dynamics simulations, DSMC simulations are subject to statistical error. To investigate the effect of the number of particles (i.e., the simulation ratio, the number of actual molecules represented by each particle), these simulations are repeated with 2–50 times the number of particles. Although the final density profiles are not identical to those from the simulations with the smaller number of particles, the numbers of bubbles and spikes are unchanged. This suggests that the most unstable wavelength determined from a simulation is not a function of the simulation ratio. A small effect of the simulation ratio is observed only when the number of particles per cell becomes so small that the statistical representation of the gas is unacceptable. Similarly, simulations initializing the random number generator with different seeds produce the same number of bubbles and spikes.

Figure 9 presents the maximum amplitude growth, defined as the distance between the highest point of helium penetration into argon and the lowest point of argon penetration into helium,

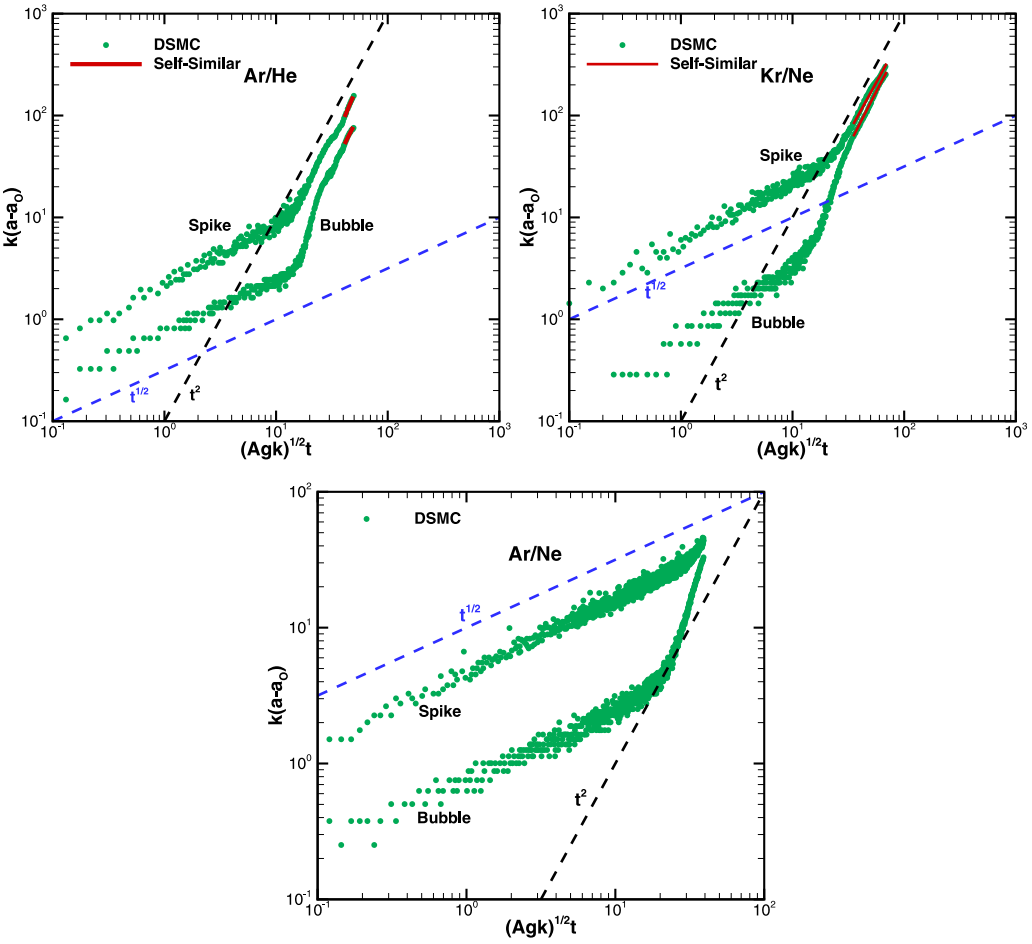

FIG. 10. Effect of Atwood number on amplitude growth for cases 4a–4c in Fig. 8, which have initially flat interfaces, illustrating when these cases enter the self-similar regime.

normalized by the most unstable wavelengths for cases 4a–4c. As expected, the instability grows faster with increasing Atwood number. For cases 4a and 4b, the cases with the two highest Atwood numbers, the interface grows enough to enter the self-similar regime. For case 4c, the interface grows due to diffusion up to the point at which it interacts with the upper and lower domain boundaries, so self-similar behavior cannot be observed. In Fig. 9 the solid curves are curve fits for the self-similar regime. Here case 4a has $\alpha^b = 0.0382$ and $\alpha^s = 0.1050$ and case 4b has $\alpha^b = 0.0600$ and $\alpha^s = 0.0661$ (case 4c does not enter the self-similar regime). The bubble values appear to be in line with expectations from experimental data [26,46–48].

Figure 10 presents the results of Fig. 9 in a log-log format to better illustrate if and when these cases begin to enter the self-similar regime. At early times, cases 4a–4c exhibit a growth proportional to $t^{1/2}$, which is characteristic of growth by diffusion. At late times, cases 4a and 4b (but not case 4c) transition to a growth proportional to t^2, as expected in the self-similar regime. This transition appears to occur around $(Agk)^{1/2}t \approx 40$, which case 4c just barely reaches.

Cherfils and Mikaelian [49] present a model explaining how viscosity and diffusivity can delay the onset of self-similar behavior until the wavelengths become relatively long, after which time self-similar behavior is recovered. This trend is clearly observed in Fig. 9, especially for case 4c with the Ar/Ne combination, which has the smallest value of Re_p.

VI. SCALING

The computational intensity of molecular methods limits the size of DSMC RTI simulations. Thus, the geometries considered here are millimeter scale, whereas many practical applications of the RTI involve larger length scales. The RTI growth can be rendered dimensionless using the most unstable wavelength λ_m, given in Eq. (1), and its exponential growth time τ, given in Eq. (4). Kadau *et al.* [50] suggest that these two quantities can be written as follows based on dimensional analysis:

$$\lambda_m = f_1(A,V)\left(\frac{\bar{\mu}^2}{g(\rho_H-\rho_L)^2}\right)^{1/3}, \tag{11}$$

$$\tau = f_2(A,V)\left(\frac{\bar{\mu}}{g^2(\rho_H-\rho_L)}\right)^{1/3}, \tag{12}$$

where $\bar{\mu} = (\mu_H + \mu_L)/2$, $V = \mu_H/\mu_L$, and f_1 and f_2 are unknown dimensionless functions of the Atwood number A and the viscosity ratio V. Through a series of molecular-level simulations, Kadau *et al.* [50] show that different RTI conditions that have equal nondimensionalized quantities are in fact equivalent. Similarly, Wei and Livescu [17] suggest the development of the RTI is strongly influenced by the perturbation Reynolds number Re_p, as defined in Eq. (3). If the most unstable wavelength were to occur at a particular numerical value $\mathrm{Re}_{p,m}$, then the following expression is obtained by substituting this value into Eq. (3) and solving for λ_m:

$$\lambda_m = \left[\left(\frac{\mathrm{Re}_{p,m}\bar{\mu}}{\rho}\right)^2 \frac{A+1}{Ag}\right]^{1/3}. \tag{13}$$

Equations (11) and (13) indicate that the most unstable wavelength depends in basically the same manner on viscosity and gravity: $\lambda_m \propto \nu^{2/3}/g^{1/3}$. With the gas pressure and temperature at STP values, setting gravity to its ambient value suggests that the results obtain herein for wavelengths of $\sim$1 mm would scale to wavelengths of $\sim$200 mm, typical of many experiments and analyses [8–12].

VII. CONCLUSION

Direct simulation Monte Carlo simulations were performed to investigate the Rayleigh-Taylor instability, in which the amplitude of an initially sinusoidal interface between two gases grows with time. Several cases were considered, including various initial perturbation wavelengths, accelerations, and gas combinations with Atwood numbers ranging from 0.32 to 0.82. The DSMC method, a molecular-level technique, enables direct observation of the role of diffusion in RTI growth from perturbed and molecularly flat interfaces.

For initially perturbed interfaces, as the perturbation Reynolds number is decreased, diffusion becomes more significant and dominates the mixing process in the early-time growth of the interface. However, the diffusive growth of the interface appears to act independently of the convective growth of the RTI, which becomes dominant as the exponential growth, due to gravitational acceleration of the flow, increases. The growth of the mixing region also shows that, although dominant in early times, diffusion does not affect the RTI significantly, thus justifying the simplifying assumptions often made in theoretical analyses of the RTI.

For flat interfaces, it was demonstrated that the molecular nature of the DSMC simulations allows the RTI to appear, triggered only by molecular fluctuations. The numbers of bubbles and spikes were found to be proportional to the numbers predicted from the most unstable wave number and to be almost equal to the numbers predicted from the most unstable wavenumber of the light gas. The statistical aspects of the simulations (simulation ratio and random number generator seed) do not affect the numbers of bubbles and spikes observed in the simulations.

The DSMC method offers a way to study hydrodynamic instabilities at the molecular level. Since DSMC inherently accounts for compressibility, viscosity, thermal conductivity, and diffusivity, it has the potential to improve the understanding of how these phenomena can influence RTI development.

The effects of internal degrees of freedom and chemical reactions on the RTI or other instabilities can also be studied straightforwardly at the molecular level.

The DSMC simulations presented herein challenge the limits of the most extreme computational platforms available. Furthermore, no visualization package currently exists that can postprocess these billion-cell, trillion-molecule data sets. Thus, we were forced to use *in situ* on-the-fly visualization, in which the physical quantities to be output are specified in advance of a run. Moreover, even on these extreme platforms, the available memory allowed only one field to be output per run. In this investigation, we selected the majority-species field because it reveals the bubbles and the spikes clearly and thus enables their growth rates to be determined. Future simulations on more powerful computational platforms will enable us to investigate the RTI in greater detail (i.e., analyzing concentration, pressure, and velocity fields).

ACKNOWLEDGMENTS

Sandia National Laboratories is a multiprogram laboratory managed and operated by Sandia Corporation, a wholly owned subsidiary of Lockheed Martin Corporation, for the U.S. Department of Energy's National Nuclear Security Administration under contract DE-AC04-94AL85000. The authors would like to thank Dr. D. J. Rader and Dr. S. N. Kempka of Sandia National Laboratories and Professor D. I. Pullin of the California Institute of Technology for many useful discussions and suggestions. SPARTA is an open-source DSMC code available from Ref. [44].

[1] W. D. Arnett, J. N. Bahcall, R. P. Kirshner, and S. E. Woosley, Supernova 1987A, Annu. Rev. Astron. Astrophys. **27**, 629 (1989).

[2] J. Lindl, Development of the indirect-drive approach to inertial confinement fusion and the target physics basis for ignition and gain, Phys. Plasmas **2**, 3933 (1995).

[3] O. A. Hurricane, D. A. Callahan, D. T. Casey, P. M. Celliers, C. Cerjan, E. L. Dewald, T. R. Dittrich, T. Döppner, D. E. Hinkel, L. F. Berzak Hopkins, J. L. Kline, S. Le Pape, T. Ma, A. G. MacPhee, J. L. Milovich, A. Pak, H.-S. Park, P. K. Patel, B. A. Remington, and J. D. Salmonson, Fuel gain exceeding unity in an inertially confined fusion implosion, Nature (London) **506**, 343 (2014).

[4] G. I. Taylor, The instability of liquid surfaces when accelerated in a direction perpendicular to their planes. I, Proc. R. Soc. London Ser. A **201**, 192 (1950).

[5] D. J. Lewis, The instability of liquid surfaces when accelerated in a direction perpendicular to their planes. II, Proc. R. Soc. London Ser. A **202**, 81 (1950).

[6] S. Chandrasekhar, The character of the equilibrium of an incompressible heavy viscous fluid of variable density, Math. Proc. Cambridge Philos. Soc. **51**, 162 (1955).

[7] L. Rayleigh, Investigation of the character of the equilibrium of an incompressible heavy fluid of variable density, Proc. London Math. Soc. **s1-14**, 170 (1883).

[8] D. H. Sharp, An overview of Rayleigh-Taylor instability, Physica D **12**, 3 (1984).

[9] F. Kull, Theory of Rayleigh-Taylor instability, Phys. Rep. **206**, 197 (1991).

[10] S. I. Abarzhi, Review of theoretical modelling approaches of Rayleigh-Taylor instabilities and turbulent mixing, Philos. Trans. R. Soc. A **368**, 1809 (2010).

[11] D. L. Youngs, Numerical simulation of turbulent mixing by Rayleigh-Taylor instability, Physica D **12**, 32 (1984).

[12] A. W. Cook and P. E. Dimotakis, Transition stages of Rayleigh-Taylor instability between miscible fluids, J. Fluid Mech. **443**, 69 (2001).

[13] J. R. Ristorcelli and T. T. Clark, Rayleigh-Taylor turbulence: Self-similar analysis and direct numerical simulations, J. Fluid Mech. **507**, 213 (2004).

[14] D. Livescu, Compressibility effects on the Rayleigh-Taylor instability growth between immiscible fluids, Phys. Fluids **16**, 118 (2004).

[15] R. E. Duff, F. H. Harlow, and C. W. Hirt, Effects of diffusion on interface instability between gases, Phys. Fluids **5**, 417 (1962).
[16] S. I. Abarzhi, A. Gorobets, and K. R. Sreenivasan, Turbulent mixing in immiscible, miscible, and stratified media, Phys. Fluids **17**, 081705 (2005).
[17] T. Wei and D. Livescu, Late-time quadratic growth in single-mode Rayleigh-Taylor instability, Phys. Rev. E **86**, 046405 (2012).
[18] G. A. Bird, *Molecular Gas Dynamics* (Clarendon, Oxford, 1976).
[19] G. A. Bird, *Molecular Gas Dynamics and the Direct Simulation of Gas Flows* (Clarendon, Oxford, 1998).
[20] M. A. Gallis, T. P. Koehler, J. R. Torczynski, and S. J. Plimpton, Direct simulation Monte Carlo investigation of the Richtmyer-Meshkov instability, Phys. Fluids **27**, 084105 (2015).
[21] O. Larroche, H. G. Rinderknecht, M. J. Rosenberg, N. M. Hoffman, S. Atzeni, R. D. Petrasso, P. A. Amendt, and F. H. Séguin, Ion-kinetic simulations of D-^{3}He gas-filled inertial confinement fusion target implosions with moderate to large Knudsen number, Phys. Plasmas **23**, 012701 (2016).
[22] D. Layzer, On the instability of superposed fluids in a gravitational field, Astrophys. J. **122**, 1 (1955).
[23] V. N. Goncharov, Analytical Model of Nonlinear, Single-Mode, Classical Rayleigh-Taylor Instability at Arbitrary Atwood Number, Phys. Rev. Lett. **88**, 134502 (2002).
[24] K. O. Mikaelian, Solution to Rayleigh-Taylor instabilities: Bubbles, spikes, and their scalings, Phys. Rev. E **89**, 053009 (2014).
[25] E. Fermi and J. von Neumann, Los Alamos Scientific Laboratory Report AECU-2979, 1953 (unpublished).
[26] V. E. Neuvazhaev, Theory of turbulent mixing, Sov. Phys. Dokl. **20**, 398 (1975).
[27] A. W. Cook, W. Cabot, and P. L. Miller, The mixing transition in Rayleigh-Taylor instability, J. Fluid Mech. **511**, 333 (2004).
[28] K. Kadau, J. L. Barber, T. C. Germann, B. L. Holian, and B. J. Alder, Atomistic methods in fluid simulation, Philos. Trans. R. Soc. A **368**, 1547 (2010).
[29] K. Kadau, T. C. Germann, N. G. Hadjiconstantinou, P. S. Lomdahl, G. Dimonte, B. L. Holian, and B. J. Alder, Nanohydrodynamics simulations: An atomistic view of the Rayleigh-Taylor instability, Proc. Natl. Acad. Sci. USA **101**, 5851 (2004).
[30] J. L. Barber, K. Kadau, T. C. Germann, P. S. Lomdahl, B. L. Holian, and B. J. Alder, Atomistic simulation of the Rayleigh-Taylor instability, J. Phys.: Conf. Ser. **46**, 58 (2006).
[31] J. Mościński, W. Alda, M. Bubak, W. Dzwinel, J. Kitowski, M. Pogoda, and D. A. Yuen, in *Annual Reviews of Computational Physics V*, edited by D. Stauffer (World Scientific Publishing Company, Singapore, 1997), p. 97.
[32] I. Sagert, J. Howell, A. Staber, T. Strother, D. Colbry, and W. Bauer, Knudsen-number dependence of two-dimensional single-mode Rayleigh-Taylor fluid instabilities, Phys. Rev. E **92**, 013009 (2015).
[33] G. A. Bird, Monte Carlo simulation of gas flows, Annu. Rev. Fluid Mech. **10**, 11 (1978).
[34] E. P. Muntz, Rarefied gas dynamics, Annu. Rev. Fluid Mech. **21**, 387 (1989).
[35] D. A. Erwin, G. C. Pham-Van-Diep, and E. P. Muntz, Nonequilibrium gas flows. I: A detailed validation of Monte Carlo direct simulation for monatomic gases, Phys. Fluids A **3**, 697 (1991).
[36] W. Wagner, A convergence proof for Bird's direct simulation Monte Carlo method for the Boltzmann equation, J. Stat. Phys. **66**, 1011 (1992).
[37] M. A. Gallis, J. R. Torczynski, and D. J. Rader, Molecular gas dynamics observations of Chapman-Enskog behavior and departures therefrom in nonequilibrium gases, Phys. Rev. E **69**, 042201 (2004).
[38] D. J. Rader, M. A. Gallis, J. R. Torczynski, and W. Wagner, DSMC convergence behavior of the hard-sphere-gas thermal conductivity for Fourier heat flow, Phys. Fluids **18**, 077102 (2006).
[39] M. A. Gallis and J. R. Torczynski, Investigation of the ellipsoidal-statistical Bhatnagar-Gross-Krook kinetic model applied to gas-phase transport of heat and tangential momentum between parallel walls, Phys. Fluids **23**, 030601 (2011).
[40] S. Chapman and T. G. Cowling, *The Mathematical Theory of Non-Uniform Gases*, 3rd ed. (Cambridge University Press, Cambridge, 1970).
[41] M. A. Gallis, J. R. Torczynski, D. J. Rader, M. Tij, and A. Santos, Normal solutions of the Boltzmann equation for highly nonequilibrium Fourier flow and Couette flow, Phys. Fluids **18**, 017104 (2006).

[42] A. L. Garcia, Nonequilibrium fluctuations studied by a rarefied-gas simulation, Phys. Rev. A **34**, 1454 (1986).

[43] K. Balakrishnan, J. B. Bell, A. Donev, and A. L. Garcia, in *28th International Symposium on Rarefied Gas Dynamics 2012*, edited by M. Mareschal and A. Santos, AIP Conf. Proc. No. 1501 (AIP, New York, 2012), p. 695.

[44] S. J. Plimpton and M. A. Gallis, SPARTA Direct Simulation Monte Carlo (DSMC) Simulator, http://sparta.sandia.gov (2015).

[45] M. A. Gallis, J. R. Torczynski, S. J. Plimpton, D. J. Rader, and T. Koehler, in *29th International Symposium on Rarefied Gas Dynamics*, edited by J. Fan, AIP Conf. Proc. No. 1628 (AIP, New York, 2014), p. 27.

[46] W. H. Cabot and A. W. Cook, Reynolds number effects on Rayleigh-Taylor instability with possible implications for type-Ia supernovae, Nat. Phys. **2**, 562 (2006).

[47] G. Dimonte and M. Schneider, Density ratio dependence of Rayleigh-Taylor mixing for sustained and impulsive acceleration histories, Phys. Fluids **12**, 304 (2000).

[48] S. B. Dalziel, P. F. Linden, and D. L. Youngs, Self-similarity and internal structure of turbulence induced by Rayleigh-Taylor instability, J. Fluid Mech. **399**, 1 (1999).

[49] C. Cherfils and K. O. Mikaelian, Simple model for the turbulent mixing width at an ablating surface, Phys. Fluids **8**, 522 (1996).

[50] K. Kadau, J. L. Barber, T. C. Germann, and B. J. Alder, Scaling of atomistic fluid dynamics simulations, Phys. Rev. E **78**, 045301 (2008).